

Die Grenzen der
Chemie neu ausloten?
It takes
#HumanChemistry

Wir suchen kreative Chemikerinnen und Chemiker,
die mit uns gemeinsam neue Wege gehen wollen –
mit Fachwissen, Unternehmertum und Kreativität für
innovative Lösungen. Informieren Sie sich unter:

evonik.de/karriere

Customizing New Titanium Dioxide Nanoparticles with Controlled Particle Size and Shape Distribution: A Feasibility Study Toward Reference Materials for Quality Assurance of Nonspherical Nanoparticle Characterization

Francesco Pellegrino,* Erik Ortel, Johannes Mielke, Roland Schmidt, Valter Maurino, and Vasile-Dan Hodoroba*

An overview is given on the synthesis of TiO₂ nanoparticles with well-defined nonspherical shapes (platelet like, bipyramidal, and elongated), with the focus on controlled, reproducible synthesis, as a key requirement for the production of reference materials with homogeneous and stable properties. Particularly with regard to the nanoparticle shapes, there is a high need of certified materials, solely one material of this type being commercially available since a few months (elongated TiO₂). Further, measurement approaches with electron microscopy as the golden method to tackle the nanoparticle shape are developed to determine accurately the size and shape distribution for such nonspherical particles. A prerequisite for accurate and easy (i.e., automated) image analysis is the sample preparation, which ideally must ensure a deposition of the nanoparticles from liquid suspension onto a substrate such that the particles do not overlap, are solvent-free, and have a high deposition density. Challenges in the synthesis of perfectly monodispersed and solvent-free TiO₂ nanoparticles of platelet and acicular shapes are highlighted as well as successful measurement approaches on how to extract from 2D projection electron micrographs the most accurate spatial information, that is, true 3D size, for example, of the bipyramidal nanoparticles with different geometrical orientations on a substrate.

antifogging coatings or self-cleaning surfaces.^[1,2] The large bandgap of TiO₂ nanoparticles confers the material a high photocatalytic activity after UV absorption, resulting finally in extraordinary material functionalities.^[3] Further remarkable applications are the ability of the decomposition of toxic organic compounds in wastewater or as efficient absorber layers in solar cells.^[4] When smaller than 50 nm, the TiO₂ nanoparticles become transparent to visible light, but block UV radiation, thus making them suitable as the defining component of sunscreen.^[5]


Depending on application, the TiO₂ particles are mostly of irregular shape, have a size range varying from a few nanometers up to several hundreds of nanometers, provide mostly anatase or rutile polymorphs (seldom also brookite), and are often coated with an ultrathin layer of silica or/and alumina.^[6,7] Agglomeration and aggregation are often encountered phenomena, particularly with ultrafine TiO₂ particles, an aspect which seems to be of high relevance in the understanding of operation of nanoparticulate TiO₂-based products.^[8,9]

To further develop new nanoenabled products with enhanced properties and understand the mechanisms underlying their superior functionalities, a detailed and accurate characterization of the physicochemical properties at the nanoscale is inherent.

1. Introduction

Titanium dioxide constitutes one of the nanoparticulate materials widely used in large-scale applications, such as an additive to housing products, high-tech construction materials paints, cements, plastics, tiles, etc., which are thus functionalized in

F. Pellegrino, V. Maurino
Dipartimento di Chimica and NIS Inter-Department Centre
University of Torino
Via P. Giuria 7, 10125 Torino, Italy
E-mail: francesco.pellegrino@unito.it

 The ORCID identification number(s) for the author(s) of this article can be found under <https://doi.org/10.1002/adem.202101347>.

© 2021 The Authors. Advanced Engineering Materials published by Wiley-VCH GmbH. This is an open access article under the terms of the Creative Commons Attribution License, which permits use, distribution and reproduction in any medium, provided the original work is properly cited.

DOI: 10.1002/adem.202101347

F. Pellegrino, V. Maurino
UniTO-ITT Joint Lab
University of Torino
via G. Quarello, 15/A, 10135 Torino, Italy

E. Ortel, J. Mielke, V.-D. Hodoroba
Division 6.1 Surface Analysis and Interfacial Chemistry
Federal Institute for Materials Research and Testing (BAM)
Unter den Eichen 44-46, 12203 Berlin, Germany
E-mail: dan.hodoroba@bam.de

R. Schmidt
Hitachi High-Tech Europe GmbH
Europark Fichtenhain A12, 47807 Krefeld, Germany

Thus, analytical methods able to measure basic nanoparticle properties such as size distribution, shape, surface area, chemical composition, surface chemistry, and crystallinity are requested. Many analytical methods able to address one or more parameters are available; however, standardized measurement procedures, including, for example, the challenging sample preparation step and uniform data analysis, are available only in singular cases.^[10] A basic issue in the reliability of the final result is the validity of the measurement method, which can be guaranteed mostly by means of comparative measurements on well-known nanoparticles as (certified) reference materials, ideally of the same chemical matrix.^[11,12] The present article intends to give an overview of the several developments of TiO₂ nanoparticles as reference materials with a focus on the morphological–structural properties, particle size, shape, and crystallinity on the background of general scarce availability of reference materials. Currently, there is a big lack of nanoparticles as certified reference materials,^[11] solely gold, silica,^[13] and polystyrene^[14] of spherical or close-to-spherical shape and monodispersed size distribution, and, recently, bimodal colloidal silica^[15] and titania elongated nanoparticles^[16] are commercially available. New measurement procedures are necessary to be codeveloped simultaneously with the controlled, reproducible synthesis of new nanoparticles as a certified reference material.^[17–21] The current known progress of such measurement approaches is also reported in this article. Initiatives and contributions to (pre-) standardized measurement procedures of nanoparticle size and shape distribution by electron microscopy (scanning electron microscopy (SEM) and transmission electron microscopy (TEM)), including interlaboratory comparisons, are presented, too.

Besides the availability of suitable nanoparticles as certified reference materials and standardized measurement procedures for the accurate size and shape analysis from the electron microscopy images, there is a need of optimized sample preparation procedures.^[11] Ideally for the subsequent analysis, a sample preparation procedure shall guarantee that the particles are not overlapped on a substrate, are solvent free, and have a high deposition density. In this case, good conditions for an automated analysis are ensured.^[22]

2. Materials and their Synthesis

In this article, we will focus our study on the synthesis and morphological (size and shape) characterization procedures of titanium dioxide nanoparticles only. We go systematically

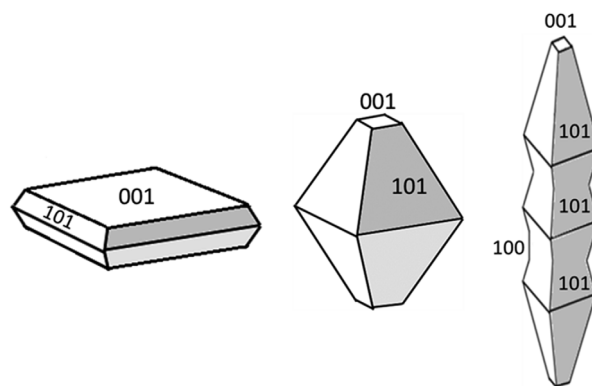


Figure 2. Schematic of TiO₂ nanoparticles highlighting their tunable crystalline shape: platelet like, bipyramidal, and elongated/acicular.

through the variety of available shapes of TiO₂ nanoparticles, so that the selected shapes are representative of nonspherical nanoparticles and also of other materials, for example, ZnO, BaSO₄, CeO₂, kaolin, etc: platelet like, bipyramidal, elongated, spherical, irregular, and strongly agglomerated/aggregated nanoparticles. The corresponding representative SEM images are shown in **Figure 1**. Of these five shapes of TiO₂ nanoparticles, the first three shapes can be considered as belonging to the same category of basic crystalline materials, but having different aspect ratios, as schematically represented in **Figure 2**. These well-defined, regular shapes of TiO₂ nanoparticles can be synthesized on a routine base in batches at laboratory scales and, with appropriate measurement procedures, constitute good candidates for nanoparticles of nonspherical shapes as reference materials. The synthesis procedures of the three types of model TiO₂ nanoparticles as in Figure 1a,b,c and 2 are described in detail in the following subsections. The description of the synthesis of spherical, polydispersed TiO₂ nanoparticles in Figure 1d by femtosecond laser ablation in water and the extensive characterization of the nanoparticle morphology and structure are given in the study by Donélienè et al.^[23] The TiO₂ nanoparticles in Figure 1e were synthesized by a sol–gel process, having targeted a high specific surface area (>150 m² g⁻¹). Their stepwise synthesis and characterization have been developed, together with the spherical particles in Figure 1d, as part of the European Union FP7 project SETNanoMetro.^[24] Both latter types of TiO₂ nanoparticles are not further addressed in this paper.

In practical applications, TiO₂ can be often found as thin and thick layers with structures at the nanoscale, either as porous

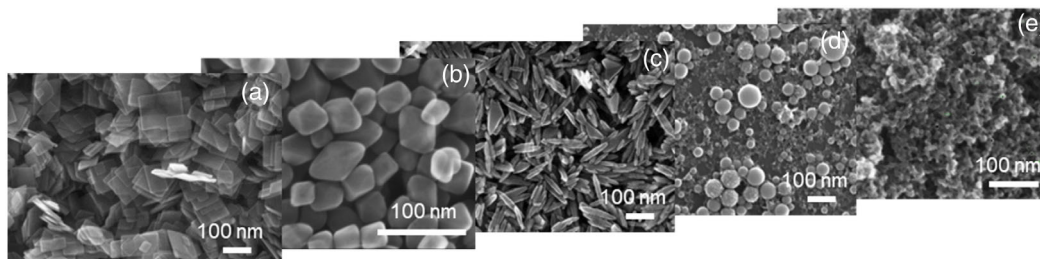


Figure 1. Various types of TiO₂ nanoparticles: a) platelet like, b) bipyramidal, c) acicular, d) spherical, and e) irregular, ultrafine, and strongly agglomerated/aggregated.

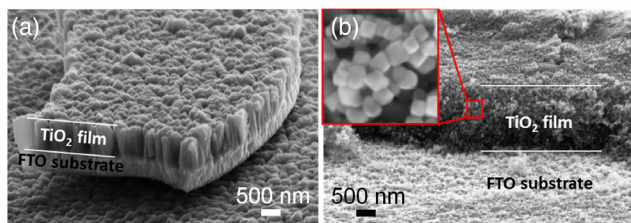


Figure 3. TiO₂ layers a) as coating synthesized by pulsed DC magnetron sputtering (after scratching it with a scalpel) and b) screen printed with the bipyramidal nanoparticles from Figure 1c as the starting material.

material or as densely packed nanoparticles, including also their functionalization.^[25,26] Two representative examples are shown in **Figure 3**. First is a TiO₂ coating synthesized by pulsed DC magnetron sputtering for photocatalysis applications, where microstructure, phase, orientation, and porosity at the nanoscale through the $\approx 1\ \mu\text{m}$ -thick layer play a decisive role.^[27,28] The second example represents a screen-printed film of a few micrometers thickness with bipyramidal nanoparticles from Figure 1c as the starting material being tested for application in a dye-sensitized solar cell, after corresponding loading with a sensitizing dye.^[29] Here, too, the morphological and crystalline structures determine the operation of this absorption layer. The synthesis and characterization of layered structures are out of the scope of this article.

2.1. Synthesis of Platelet-like TiO₂ Nanoparticles

Anatase nanoparticles with a large percentage of {001} facets have become a target in the synthesis of anatase TiO₂ crystals, since Yang et al. realized the first case of 47% (001) in uniform crystals. Synthesis procedures leading to nanoparticles (NPs) have been developed with higher {001} percentages.^[30–41]

Controlling the concentrations of precursors and fluorine species, also with the synergistic effects of other capping agents, the relative percentage of (001) surfaces can be tuned. For example, the percentage of {001} increases from 18% to 72%, decreasing the concentration of Ti(SO₄)₂ from 100 to 10 mM.^[34] Zhang et al.^[42] showed that the percentage gradually improved with increasing amount of 1-butyl-3-methylimidazolium tetrafluoroborate.

It was found that the increase in the surface coverage fractions of fluorine increase the percentage of (001). Theoretically, different surface coverage fractions can greatly affect the surface energy and thus the percentage of {001} during the growth of crystals.^[13]

Using alcohol as the synergistic capping agent, the percentage can be further improved.^[35,37]

Two other methods have also been developed to synthesize anatase nanoparticles with a high percentage of {001} facets. The first one provides the direct conversion of amorphous TiO₂ nanotube arrays on titanium foil to anatase crystals with well-defined {101} and {001} by calcining at a temperature above 673 K in air for 2 h.^[43] The other is to use a gas-phase reaction of TiCl₄ with O₂ in a nonequilibrium method with fast quenching of the system from 1473 K, as described in the preceding section.^[31] In this way, small TiO₂ particles (50–250 nm) could be

obtained at such high temperatures without using fluorine-containing reactants.

Besides fluoride, other shape controllers were proposed to grow anatase nanoparticles with high exposition of {001} surfaces. Chen et al. proved that diethylenetriamine in isopropyl alcohol could act as an alternative morphology controlling agent in a solvothermal system.^[44] The freshly prepared TiO₂ microspheres consisting of {001} dominant sheets are poor in crystallinity. Postcalcination at 673 K in air leads to increased crystallinity without morphology change.

In this work, figures and analysis are referred to platelet-like nanoparticles (see Figure 1a) obtained by a solvothermal method in which pure titanium *t*-butoxide is used as Ti precursor and hydrofluoric acid (HF) as capping agent. The synthesis of this material was exhaustively discussed in previous works.^[45,46]

2.2. Synthesis of Bipyramidal TiO₂ Nanoparticles

{101} facets dominate the surface of most anatase nanoparticles.^[47] Through the Ostwald ripening of amorphous hydrated TiO₂, it is possible to obtain regular {101} facets. As early as 1999, lightly truncated bipyramidal crystals with well-defined {101} surfaces were synthesized by coarsening pristine titania particles using sol–gel routes under various hydrothermal conditions.^[48] The percentage of (101) can be varied by changing the growth rates along <001> and <101> directions during different growth stages. In all cases, the driving force is the reduction in surface energy. Minimizing the presence of high-energy surfaces allows reducing surface energy, inducing morphology evolution. Recently, approaches using titanates as feeders have been reported to obtain anatase with a high percentage of {101}. Ohtani and co-workers^[49,50] reported hydrothermal transformation directly from potassium titanate nanowires to bipyramidal anatase single crystals with a predominant {101} surface.

The role of the water in promoting the growth of bipyramidal nanoparticles that largely expose the {101} facets in acidic or neutral media is confirmed by Liu et al.,^[51] who obtained anatase bipyramids by treating at 453 K a suspension of amorphous Ti(OH)₄ in water/ethanol solution. They proposed to control the shape of the final anatase nanoparticles by adding a capping reagent able to control the crystal growth. The presence of fluorides increases the truncation level of the bipyramids, increases the amount of {001} surface to 30–40%, whereas sulfates allow to synthesize nanorods with high percentage of (100) facets. Using oxalate and lactate, the solvothermal treatment leads to rutile and brookite nanorods, respectively.

Dai et al.^[30] used small particles of amorphous TiO₂ obtained by electrospinning as precursor to prepare truncated bipyramids of anatase via a hydrothermal route. Low pH leads to percentages of {101} near 90%.

Recently, the reproducible preparation of anatase bipyramids with high percentage of {101} exposed was achieved by the hydrothermal treatment of Ti(IV)-triethanolamine complex aqueous solution at 423–483 K.^[52,53] Variation of the temperature allows the control of particle size. At 453 K, uniform bipyramids with 20 nm hydrodynamic radius are obtained. The synthesis of the bipyramidal nanoparticles considered in this work (see Figure 1b) has been carried out with this last method, as described in several papers.^[45,53,54]

2.3. Synthesis of Acicular TiO₂ Nanoparticles

The synthesis of acicular TiO₂ nanoparticles is not common as other shapes. Usually, elongated morphologies such as nanotubes or rods are described for several applications.^[55,56] The synthesis of small acicular nanoparticles is tricky, especially if the desired facet is the {100}.^[51]

Li et al. used sodium titanate nanotubes to prepare uniform anatase nanorods with a large percentage of (010) facet by a hydrothermal process in basic solution.^[57] The proposed growth mechanism involves the formation of Ti(OH)₄ fragments from titanate nanotubes and subsequent anatase crystal nuclei by the dehydration reaction between Ti–OH and HO–Ti. The continuous release of OH[−] during the hydrothermal process plays a key role in generating (010) facets. Barnard et al.^[58] showed that O-terminated (010) had a lower surface energy than O-terminated (101) and (001). It was believed that the preferential adsorption of the hydroxyl ion on (010) face contributed to stabilizing the (010) faces.

By controlling carefully the preparation parameters, Pan et al. prepared anatase single crystals with a predominance of {101}, {001}, and {010}, respectively. The syntheses are carried out by mixing different amounts of HF solutions (120, 80, and 40 mM) with different quantities of TiOSO₄ precursors (64, 32, and 32 mg) and heating at 453 K for 12, 12, and 2 h, respectively.^[38]

Dinh et al. also reported routes to prepare anatase crystals in various shapes.^[59] In their approach, the use of water vapor as the hydrolysis agent to accelerate the reaction is crucial, together with the use of both oleic acid and oleylamine as capping surfactants. Different shapes such as rhombic, truncated rhombic, spherical, dog bone, truncated, and elongated rhombic and bars could be synthesized. Although the authors did not identify crystallographic facets of the exposed surface, it is possible to conclude, based on the symmetries and predicted morphologies of anatase, that the elongated crystals expose (010) facets.

Pellegrino et al., through the use of combined experimental design and machine learning techniques, were able to modulate and predict the nanoparticles characteristics given the synthesis parameters.^[53] Similar to the bipyramid case, the synthesis is a hydrothermal treatment of Ti(IV)-triethanolamine complex in an aqueous solution. They found that high pH values and low temperatures are able to favor the growth of the nanoparticles along the *c*-axis, resulting in high-aspect-ratio nanoparticles. The acicular nanoparticles taken into consideration in this manuscript (Figure 1c) were synthesized with the same method described by Pellegrino et al.^[53] The presence of high-energy facets in these kinds of nanoparticles is very low; see the high-resolution image in Figure 4. They mainly expose {101} surfaces grown on on each other in very short sequences, so that the final shape becomes elongated/acicular, not having a well-defined simple shape like rod or bipyramid.

3. Results and Discussion

In this section, optimized procedures for the accurate measurement of the size and shape of the selection of the three types of TiO₂ nanoparticles will be presented and discussed. Challenges in the extraction of 3D information of nonspherical particles

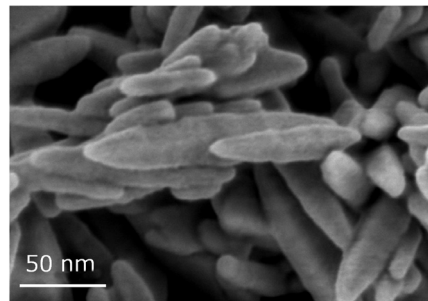


Figure 4. High-resolution SEM image with the acicular TiO₂ nanoparticles considered in this work.

from 2D projection electron microscopy images and ways of alleviating them are proposed. The analysis of the bipyramidal nanoparticles is treated with extensive details due to the representativity of the bipyramidal shape for nonspherical nanoparticles. Special attention is paid to sample preparation protocols. Particularly, for the purpose of evaluation of the accurate dimensional parameters' size and shape of nonspherical nanoparticles by means of electron microscopy, the deposition of nanoparticles from a liquid suspension onto a substrate as nonoverlapped particles, without additional contamination or solvent rests, and with a high density on the substrate, is a key prerequisite. Ideally, a monolayer of nonoverlapping nanoparticles ensures the highest analysis efficiency. As shown in the next subsections, each type of material presents its own preparation challenges, but finally optimized protocols ensure not only accurate analysis but also enable its easy automation.^[59,60]

3.1. Platelet-like TiO₂ Nanoparticles

Generally, nanoplatelets are difficult to be deposited on a substrate as single particles, independent of the material type, for example, kaolin,^[61] TiO₂,^[62] or graphene,^[63] which is usually strongly agglomerated/aggregated (along their large faces). The TiO₂ nanoplatelets as deposited from liquid suspension on a carbon TEM grid according to an optimized sample preparation procedure are described in Section 5. Experimental Section is described in Figure 5. A significant fraction of the platelets is deposited as single particles; however, the largest fraction of platelets can be observed (in both SEM operating modes) as agglomerates of a few stapled particles, which can barely (or impossible) be completely separated in single particles by further preparation methods. Practically, all nanoplatelets are parallel with the substrate, making the accurate measurement of the most relevant dimension, that is, their thickness, impossible with a conventional SEM. The number of overlapped nanoplatelets can be just roughly estimated as long as the stapled nanoplatelets are only a few. Buhr et al.^[64] demonstrate an approach of determining the nanoparticle thickness, however, no platelets, based on the physical modeling of the electron scattering processes underlying the STEM-in-SEM signals and preknowledge on the nanomaterial.

In summary, the accurate measurement of nanoplatelets is possible but with respect to the lateral dimensions (of

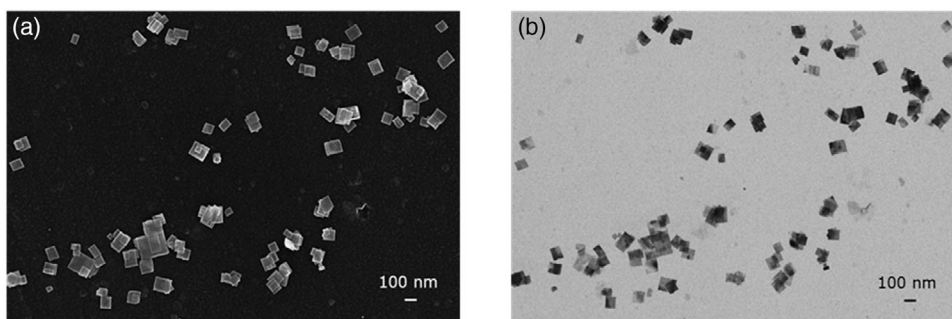


Figure 5. a) SEM and b) STEM-in-SEM micrographs of same field of view with TiO_2 nanoplatelets as deposited on a carbon film TEM grid from liquid suspension.

50–60 nm) only. Neither the size distribution of the particle's lateral dimensions is highly monodisperse, nor the shape of the platelets is perfectly square like. For these reasons, despite good progress with the preparation and analysis procedures, this type of material is currently not further considered to be certified as a reference material.

One approach which relatively easily helps in the determination of the smallest dimension of nanoplatelets is dry preparation as powder on a substrate, with the advantage of no additional sample preparation or risk of having rests of solvent. If prepared on an electron-transparent substrate, a pair of images SEM/STEM-in-SEM at a “lucky” location as in **Figure 6** can be recorded, where one or more staples of nanoplatelets are oriented perpendicular to the substrate. In this case, the thickness of the nanoplatelets becomes accessible in an SEM and a mean value of

about 10 nm for all stapled platelets could be measured with both working modes SEM and STEM-in-SEM.

3.2. Bipyramidal TiO_2 Nanoparticles

The most relevant type of nanoparticle selected in this article as being representative for nonspherical nanoparticles is the case of bipyramidal TiO_2 nanoparticles. At the first sight, the measurement of their dimensions might look like an easy task. The practice shows that a rough estimation of the nanoparticle sizes is possible under the prerequisite that a high-resolution SEM is available. An example of such high-quality micrographs offering details on the nanoparticle morphology at the nanometer scale is given in **Figure 7**, with a representative pair of images SEM and STEM-in-SEM after sample preparation from liquid suspension

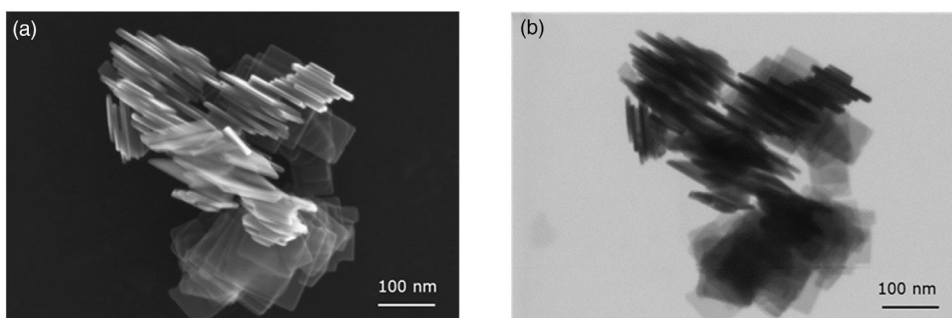


Figure 6. a) SEM and b) STEM-in-SEM micrographs of same field of view with TiO_2 nanoplatelets as deposited on a carbon film TEM grid as dry powder.

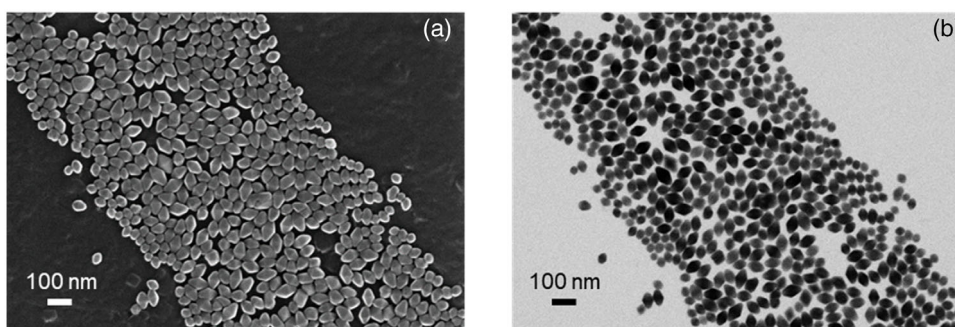


Figure 7. a) SEM and b) STEM-in-SEM micrographs of same field of view with bipyramidal TiO_2 nanoparticles as deposited on a carbon film TEM grid.

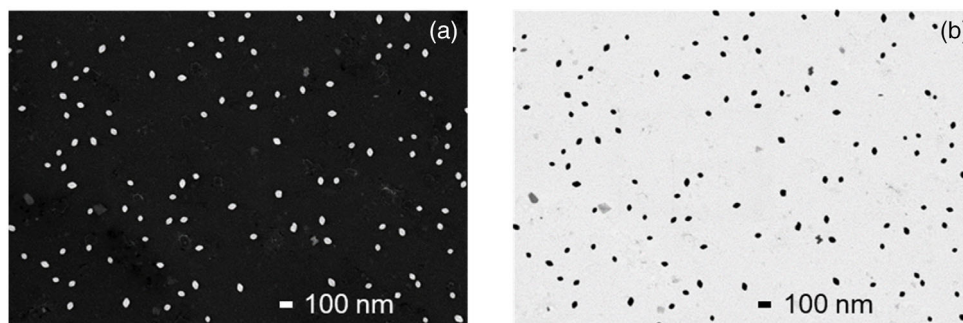


Figure 8. a) SEM and b) STEM-in-SEM micrographs of same field of view with bipyrarnidal TiO_2 nanoparticles as deposited on a carbon film TEM grid after the optimized sample preparation procedure.

on a carbon TEM grid. Following the first, qualitative observations can be drawn. 1) Practically all the particles are of bipyrarnidal shape with lengths of about 40–70 nm and widths of 20–50 nm; 2) The larger particles are bordered by smaller particles (the pair of images in Figure 7 is representative) for this type of material; 3) The high-resolution, secondary electrons' (SEs) InLens micrograph offers more details on the shape of the nanobipyramids, as deposited on the substrate. It should be noticed that the geometrical orientation of the bipyramids as deposited in this case either lies on a particle facet or lies parallel with the substrate. Exact quantification approaches are given in detail in the study by Crouzier et al.^[65]; and 4) The superior contrast of STEM-in-SEM with respect to the mass thickness contrast enables a more accurate reading of the particle boundaries, however, without knowledge of the exact 3D orientation of the particles on the substrate. Correlative approaches such as SEM and atomic force microscopy (AFM) or SEM with STEM-in-SEM and transmission Kikuchi diffraction (TKD)^[65,66] have a decisive contribution in extracting accurate full 3D information of the nonspherical nanoparticles.

Like the other types of nonspherical nanoparticles, a corresponding deposition procedure from liquid suspension is developed/optimized, as described in Section 5. In Experimental Section, the nanoparticle distribution on the substrate is very homogeneous, as shown in Figure 8. Thus, for these types of nanoparticles, the deposition of only single particles was attained, and this enables, hence, an automated particle analysis based on a set of such images.

Once having a deposition of the bipyrarnidal TiO_2 nanoparticles as close as possible to the monolayer, the image segmentation defined by appropriate thresholding can proceed and the particles can be counted and analyzed automatically with respect to a large series of size and shape descriptors at high throughput. Especially the STEM-in-SEM or conventional TEM projection images are well suited for accurate dimensional analysis of nanoparticles. Figure 9 shows representatively the sequence of image analysis from 1) the raw STEM-in-SEM image, to 2) after binarization, to 3) automated identification of and analysis of the particles, and up to 4) the manual correction of artifacts like agglomerated particles being identified as one larger particle. Once again, the preparation step providing nonagglomerated/overlapped particles is decisive for the automated analysis. The image analysis sequence is usually carried out with

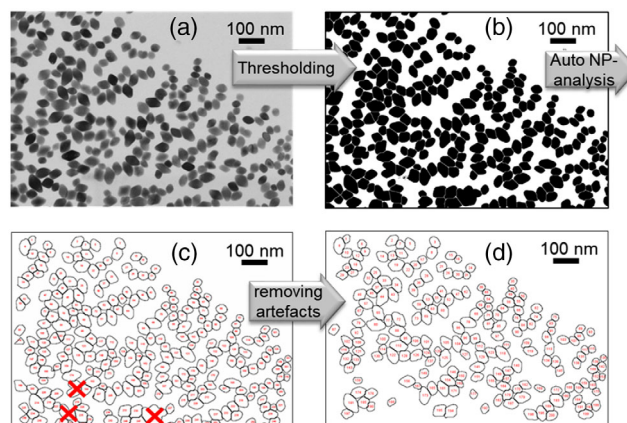


Figure 9. Workflow with the TSEM-in-SEM image analysis of bipyrarnidal TiO_2 nanoparticles as deposited on a carbon film TEM grid: a) raw STEM-in-SEM micrograph, b) result of thresholding of a,c) automatic particle analysis in the image. b,d) Final counted particles after excluding artefacts due to agglomeration.

ImageJ,^[67] a freeware software which is intuitively and rich in options regarding the type of size and shape of descriptors to be calculated and reported. The final result of the data analysis of the images as in Figure 9 but for 508 nanoparticles is shown in Figure 10. Of the many easily possible attainable size and shape descriptors provided by ImageJ, the maximum feret diameter (denominated “feret diameter” in ImageJ), the minimum feret, and the aspect ratio were identified for this type of sample as the most relevant. Other descriptors like area, equivalent circular diameter, roundness, elliptical diameter/major axis, elliptical diameter/minor axis, perimeter, equivalent perimeter diameter, ellipse ratio, extent, bulkiness, circularity, compactness, perimeter of the convex hull envelope, convexity, area of convex hull envelope, solidity, and ruggedness can be easily extracted when necessary.

For the case of titania nanoparticles of more complex shapes, the automated analysis cannot be applied anymore, and manual analysis is the current state. Grulke et al.^[68] reported extensively, with examples for each image analysis step, how exactly such a case shall be treated. Both representative examples, bipyrarnidal

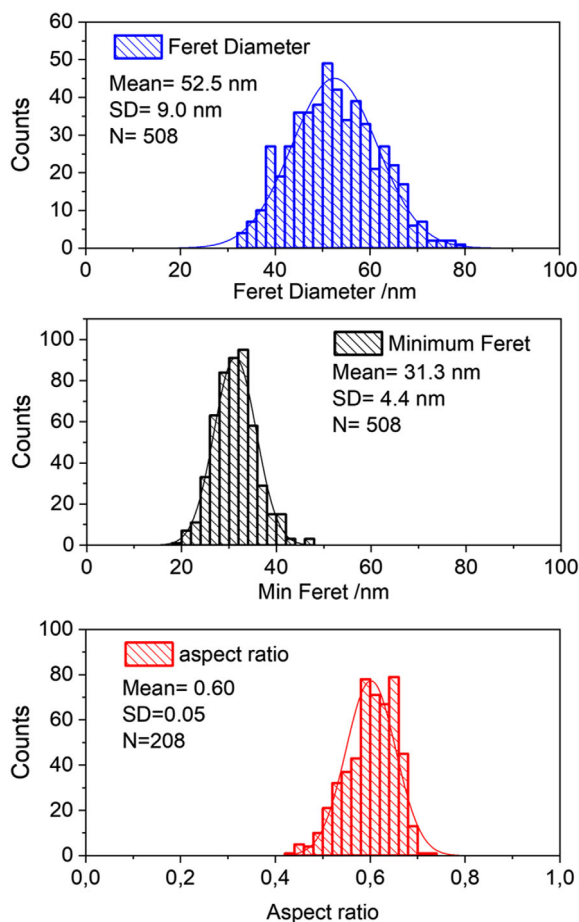


Figure 10. Results of the STEM-in-SEM image analysis of 508 bipyramidal TiO_2 nanoparticles according to the workflow shown in Figure 9 for the three size and shape descriptors, maximum feret diameter (same with “feret diameter” in ImageJ), the minimum feret, and the aspect ratio.

and irregular aggregated TiO_2 nanoparticles, were selected for interlaboratory comparisons under the standardization committee ISO/TC 229 Nanotechnologies (www.iso.org/committee/381983.html), and the two case studies have been included as the case studies F-nanocrystalline aggregates and

H-nanoparticles with specific crystal habits.^[69] Very recently, a corresponding ISO standard addressing a case study on TiO_2 nanoparticle size measurement has been published.^[70] The measurement procedures as described in this article are in line with these two ISO standards. The results of an interlaboratory comparison on these types of samples have been reported in ISO 21 363:2020 as follows.^[69] The average value of the maximum feret diameter from 14 laboratories was 51.2 nm with a standard deviation of 3.19 nm (6.24%), and the average minimum feret diameter was 32.8 nm with a standard deviation of 4.45 nm (4.13%). Note that the 14 laboratories have used various versions of transmission electron microscopies, that is, TEM, STEM-in-SEM, and also the so-called “mini-TEM” instrumentation. Such a small standard deviation of about 5% indicates an excellent performance of TEM-based techniques to measure the size and shape of such a relative complex nanoparticulate material. It should be noticed, however, that the quality of the sample preparation is mostly the major source of uncertainty. Strong agglomeration/overlapping of particles or improper separation of the nanoparticles from solvent or contamination can affect considerably the accuracy of size measurement by poor or impossible distinction of individual nanoparticles; also the representativity of measurement is strongly affected. Further, the calibration of the pixel size, together with the image resolution (in pixels), goes also into the measured dimension of each particle. Particularly in the STEM-in-SEM mode, where the resolution is poorer than in a conventional TEM, the setting of the true threshold for image segmentation (separation of the particles from background) can induce significant errors. This threshold value is dependent on material, beam energy, and nanoparticle size. Published values derived from physical modeling on selected systems can be considered^[64] or, more practically, the use of as-similar-as-possible nanoparticulate certified reference materials.

Alternative to the drop-cast deposition procedure from liquid suspension, if powder with the same nanoparticles is available, the dry preparation of the sample on a usual SEM substrate is possible for SEM analysis. An example is shown in **Figure 11**. The excellent morphology contrast enables the identification of many of the visualized bipyramidal nanoparticles. A small software program has been developed in our laboratory with the purpose of the manual reconstruction of truncated bipyramidal nanoparticles based on such high-resolution images, as shown in Figure 11. Three angular degrees of freedom and 3D

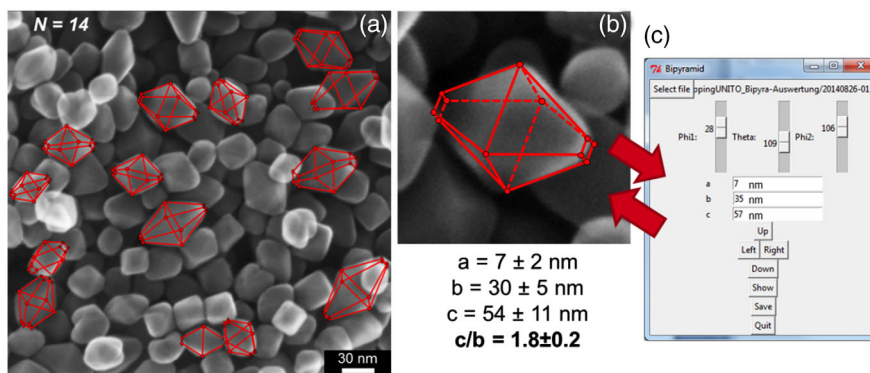


Figure 11. Workflow with the SEM image analysis of bipyramidal TiO_2 nanoparticles as deposited as dry powder on an SEM aluminum sample holder.

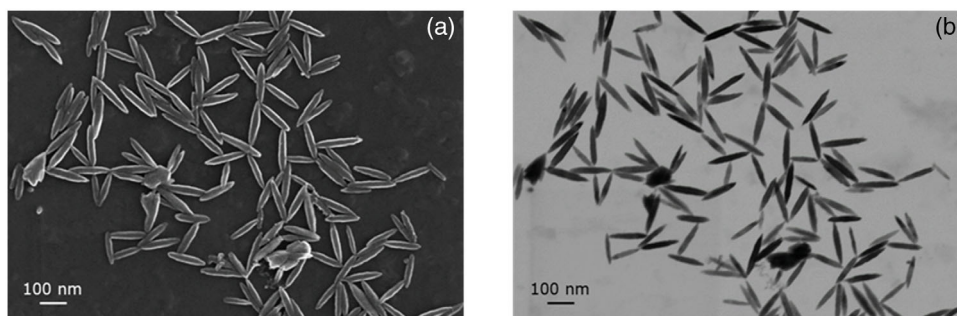


Figure 12. a) SEM and b) STEM-in-SEM micrographs of same field of view with elongated TiO₂ nanoparticles as deposited on a carbon film TEM grid after application of an optimized sample preparation procedure.

parameters (length, basal width, and truncation width at the peaks) are allowed to be manually adjusted until the match of an overlapped truncated bipyramid is visually satisfactory. As it is at this moment, the use of such an approach is time-consuming and not to be further considered as a routine approach. Nevertheless, for a reduced number of nanoparticles, the agreement with the data from the previous automated procedure (with higher statistics) is excellent.

3.3. Elongated TiO₂ Nanoparticles

Following a similar deposition procedure as for the TiO₂ nanoplatelets, the TiO₂ elongated nanoparticles were prepared for analysis with dual electron microscopy, that is, high-resolution SEM and by the transmission mode STEM-in-SEM; see a representative pair of images in **Figure 12**. Despite the relatively successful deposition as single nanoparticles of the roughly monodispersed size distribution, that is, ≈ 150 nm length and ≈ 20 nm width, reproducible narrow monodispersed synthesis of elongated TiO₂ nanoparticles could not be obtained; either a significant fraction of nonacicular structures (brookite) has been observed (better visible in the transmission mode in **Figure 12b**) or significant solvent rests have impeded at this stage the initiation of a certification process of these types of particles as reference materials. Moreover, it should be noticed that a certified reference material of the same matrix (TiO₂), of roughly similar particle shape and quality, is made commercially available.^[16] The exact morphological and structural characterization of this type of material remains complex; see the detailed description of **Figure 2c** and **4**.

4. Conclusion and Outlook

The state of the art in the measurement of the size and shape distribution of nanoparticles of nonspherical shapes with electron microscopy, based on model TiO₂ nanoparticles, is presented including limitations, challenges, but also new approaches. Recent developments with respect to notable successes in international standardization activities in measurement procedures of nanoparticles sizes and shape distribution with electron microscopy are also described. Three representative shapes of TiO₂ nanoparticles have been selected: platelet like,

bipyramids, and elongated/acicular, with the basic idea to conduct a systematic feasibility study on the reproducible synthesis of these types of nanoparticles, as well as on the detailed dedicated protocols developed for sample preparation, measurement, and data analysis. The main focus is kept on the systematic characterization of bipyramidal TiO₂ nanoparticles as a representative case of nonspherical nanoparticles. The certification procedure of TiO₂ bipyramids in compliance with the standard ISO 17 034 is planned for the next future to be carried out at BAM. As far as the TiO₂ nanoplatelets are regarded, their morphological characterization poses considerable challenges in finding a reproducible and representative size measurement procedure, particularly for the thickness as the smallest dimension. The approach followed here to develop a sample preparation protocol able to guarantee the distribution of single nanoplatelets deposited parallel onto a substrate succeeded only partially. Further developments in both directions, 1) measurement of nanoplatelet thickness in SEM-in-STEM based on the mass-thickness determination,^[64] and/or correlative analysis with AFM;^[65] and 2) representative, that is, statistical measurement of the arbitrarily oriented nanoplatelets in powder form in the SEM mode, are necessary. Artificial intelligence approaches for the automated and reliable identification and size analysis of the nanoplatelets could help to resolve this task. Further, the synthesis of TiO₂ nanoplatelets in the present work has been optimized toward monodispersed size distribution. This target could not be reached completely. The ideally perfect nanoparticle size and shape monodispersity would have simplified considerably the accurate measurement. However, a significant number of real nanoparticulate materials needing accurate morphological characterization as a routine procedure are of nanoplatelet shape. From this perspective, the TiO₂ nanoplatelets as presented in this article are rather attractive candidate reference materials. In other words, the material developed is good enough for certification purposes; however, the measurement procedures must be developed further to enable reliable thickness measurement, even for overlapped particles. In the case of elongated TiO₂ nanoparticles, the main issues lay in an irreproducible synthesis of particles with narrow monodispersity due to either a significant fraction of nonacicular structures (brookite) and/or a significant presence of solvent rests after deposition on a substrate. Other materials such as gold nanocubes and nanorods with excellent size monodispersity or bimodal silica and gold with controlled

size and the latter ones also with controlled number concentrations are promising with respect to their suitability as reference materials.^[71]

5. Experimental Section

Experimental Work: All images in this article apart of that in Figure 4 were obtained with an SEM of type Zeiss Supra 40 (Zeiss, Oberkochen, Germany), equipped with a Schottky-type cathode and an InLens detector for the so-called SE1 electrons, that is, those SEs emitted exactly (only) at the impact point of the primary beam, having a dual-working mode SEM/STEM-in-SEM (or TSEM). The advantages of working with two types of correlative imaging methods were described in detail in the study by Hodoroaba et al.^[72] Basically, the SE1 InLens detection ensured high-resolution morphological information, with very high surface sensitivity; the imaging in the transmission mode (of same field of view with the same particles as in SEM but prepared on an electron transparent substrate) provided a superior material (mass thickness) contrast suited to dimensional, projection measurements of nanoparticles with high accuracy. As a disadvantage of the transmission mode, one lost details on the exact location of the observed structures in the depth. In turn, the conventional SE imaging mode suffered from more or less signal saturation at the edges of the structures, which led mostly to an overestimation of the nanoparticle size. The image with the highest resolution (Figure 4) was taken with a Hitachi Cold FESEM SU8230 (Hitachi High-Technologies Europe GmbH, Krefeld, Germany) at 500 V, as an experimental high-resolution setup equipped with cold field emission, specimen exchange chamber, zone UV cleaning, and cold trap.

Platelet-like TiO₂ Nanoparticles: The carbon-coated TEM grid (Plano EM, S160) was hydrophilized by ozone treatment under ambient conditions with 4 W at 254 nm for 30 min (UV Ozone Cleaner UVC-1014 from NanoBioAnalytics), at an HF peak output power of 120/240 W/period. 2 mL nanoparticle suspension was ultrasonicated for 30 min using an ultrasound bath (Bandelin Sonorex RK 102 P) at room temperature without additional heating. The TEM grid was, with the carbon film side up, fixed on a thin microscope slide using a parafilm (Pechiney Plastic Packaging Inc.) 8 μ L of the sonicated suspension was drop cast onto the grid. The specimen was subsequently spin coated at 10 000 rpm for 10 min (SPS Europe, POLOSTM).

Bipyramidal TiO₂ Nanoparticles: The carbon-coated TEM grid (Plano EM, S160) was hydrophilized by ozone treatment under ambient conditions with 4 W at 254 nm for 30 min (UV Ozone Cleaner UVC-1014 from NanoBioAnalytics). 2 mL nanoparticle suspension was sonicated in an ultrasonication bath (Bandelin Sonorex RK 102 P) for 15 min, at an HF peak output power of 120/240 W/period. 6 μ L of an aqueous 1 mg mL⁻¹ poly-L-lysine hydrobromide solution was drop cast onto the grid. After 15 s, excessive solution was washed away by dipping the grid into water and, subsequently, blotting residual liquid with filter paper. After that, 6 μ L of the 50-fold diluted nanoparticle suspension was drop cast onto the grid. Then, the grid was covered with a lid to avoid evaporation and left for incubation for 30 min at room temperature. Subsequently, excessive nanoparticle suspension was washed away by dipping the grid into water and blotting residual liquid with filter paper.

Elongated TiO₂ Nanoparticles: The deposition procedure was identical with that for platelet-like TiO₂ nanoparticles; see earlier.

It should be noticed that other dedicated approaches for the sample preparation of nanoparticles are also reported in the literature, for example, using electrospray deposition,^[73] embedding the dry nanoparticles and analyzing the polished cross-sectional sample^[74] or using a dispenser.^[75,76]

Acknowledgements

This project 17NRM04 nPSize received funding from the EMPIR programme cofinanced by the Participating States and from the

European Union's Horizon 2020 research and innovation programme. Mrs. Sigrid Benemann (BAM) is greatly acknowledged for her tireless support with the acquisition of the high-resolution images. Many thanks are also due to Dr. Ulrich Mansfeld (BAM) for the development of sample preparation protocols.

Open access funding enabled and organized by Projekt DEAL.

Conflict of Interest

The authors declare no conflict of interest.

Data Availability Statement

Data sharing is not applicable to this article as no new data were created or analyzed in this study.

Keywords

nanoparticles, particle size and shape distributions, reference materials, standardizations, titanium dioxide

Received: September 30, 2021

Revised: November 3, 2021

Published online:

- [1] X. Chen, S. S. Mao, *Chem. Rev.* **2007**, *107*, 2891.
- [2] T. L. Thompson, J. T. Yates, *Chem. Rev.* **2006**, *106*, 4428.
- [3] A. Fujishima, T. N. Rao, D. A. Tryk, *J. Photochem. Photobiol., C* **2000**, *1*, 1.
- [4] B. O'Regan, M. Gratzel, *Nature* **1991**, *353*, 737.
- [5] A. P. Gondikas, F. von der Kammer, R. B. Reed, S. Wagner, J. F. Ranville, T. Hofmann, *Environ. Sci. Technol.* **2014**, *48*, 5415.
- [6] A. M. El-Toni, S. Yin, T. Sato, *J. Colloid Interface Sci.* **2006**, *300*, 123.
- [7] V. Ganapathy, B. Karunakaran, S.-W. Rhee, *J. Power Sources* **2010**, *195*, 5138.
- [8] Z. E. Allouni, M. R. Cimpan, P. J. Hølb, T. Skodvin, N. R. Gjerdet, *Colloids Surf., B* **2009**, *68*, 83.
- [9] Y. Reches, K. Thomson, M. Helbing, D. S. Kosson, F. Sanchez, *Constr. Build. Mater.* **2018**, *167*, 860.
- [10] V. A. Demin, V. F. Demin, Yu. P. Buzulukov, P. K. Kashkarov, A. D. Levin, *Nanotechnol. Russ.* **2013**, *8*, 347.
- [11] T. P. J. Linsinger, G. Roebben, C. Solans, R. Ramsch, *Trends Anal. Chem.* **2011**, *30*, 18.
- [12] A. A. Lizunova, E. G. Kalinina, I. V. Beketov, V. V. Ivanov, *Meas. Tech.* **2014**, *57*, 848.
- [13] A. Braun, V. Kestens, K. Franks, G. Roebben, A. Lamberty, T. P. J. Linsinger, *J. Nanopart. Res.* **2012**, *14*, 1021.
- [14] N. Farkas, J. A. Kramar, *J. Vac. Sci. Technol.* **2020**, *38*, 023211.
- [15] V. Kestens, G. Roebben, J. Herrmann, Å. Jämting, V. Coleman, C. Minelli, C. Clifford, P. De Temmerman, J. Mast, L. Junjie, F. Babick, H. Cölfen, H. Emons, *J. Nanopart. Res.* **2016**, *18*, 171.
- [16] V. Kestens, T. Gerganova, G. Roebben, A. Held, *Anal. Bioanal. Chem.* **2021**, *413*, 141.
- [17] J. M. Hughes, P. M. Budd, A. Grieve, P. Dutta, K. Tiede, J. Lewis, *J. Appl. Polym. Sci.* **2015**, *132*, 42061.
- [18] R. Grombe, J. Charoud-Got, H. Emteborg, T. P. J. Linsinger, J. Seghers, S. Wagner, F. von der Kammer, T. Hofmann, A. Dudkiewicz, M. Llinas, C. Solans, A. Lehner, G. Allmaier, *Anal. Bioanal. Chem.* **2014**, *406*, 3895.

- [19] S. Gu, J. Kaiser, G. Marzun, A. Ott, Y. Lu, M. Ballauff, A. Zaccone, S. Barcikowski, P. Wagener, *Catal. Lett.* **2015**, *145*, 1105.
- [20] R. You, M. Li, S. Guha, G. W. Mulholland, M. R. Zachariah, *Anal. Chem.* **2014**, *86*, 6836.
- [21] C. Rehbock, J. Jakobi, L. Gamrad, S. van der Meer, D. Tiedemann, U. Taylor, W. Kues, D. Rath, S. Barcikowski, *Beilstein J. Nanotechnol.* **2014**, *5*, 1523.
- [22] R. Grombe, G. Allmaier, J. Charoud-Got, A. Dudkiewicz, H. Erteborg, T. Hofmann, E. Huusfeldt Larsen, A. Lehner, M. Llinàs, K. Loeschner, K. Mølhave, R. J. Peters, J. Seghers, C. Solans, F. von der Kammer, S. Wagner, S. Weigel, T. P. J. Linsinger, *Accredit. Qual. Assur.* **2015**, *20*, 3.
- [23] J. Donélienè, M. Rudzikas, S. Rades, I. Dörfel, B. Peplinski, M. Sahre, F. Pellegrino, V. Maurino, J. Ulbikas, A. Galdikas, V.-D. Hodoroaba, *Mater. Res. Express* **2018**, *5*, 045015.
- [24] <http://www.metecnetwork.eu/setnanometro-project/index.html> (accessed: November 2021).
- [25] S. Rades, P. Borghetti, E. Ortel, T. Wirth, M. Blanco, E. Gómez, A. Martinez, J. Jupille, G. Martra, V.-D. Hodoroaba, *Surf. Interface Anal.* **2018**, *50*, 1200.
- [26] V.-D. Hodoroaba, S. Rades, P. Borghetti, E. Ortel, T. Wirth, S. Garcia, E. Gómez, M. Blanco, G. Alberto, G. Martra, *Surf. Interface Anal.* **2020**, *52*, 829.
- [27] E. Ortel, I. Häusler, W. Österle, S. Narbey, F. Oswald, I. H. Andersen, M. Holzweber, W. E. S. Unger, V.-D. Hodoroaba, *Surf. Interface Anal.* **2016**, *48*, 664.
- [28] E. Ortel, A. Hertwig, D. Berger, P. Esposito, A. M. Rossi, R. Kraehnert, V.-D. Hodoroaba, *Anal. Chem.* **2016**, *88*, 7083.
- [29] S. Rades, F. Oswald, S. Nerbey, J. Radnik, V.-D. Hodoroaba, *Surf. Interface Anal.* **2018**, *50*, 1234.
- [30] Y. Dai, C. M. Coble, J. Zeng, Y. Sun, Y. Xia, *Nano Lett.* **2009**, *9*, 2455.
- [31] F. Amano, O. O. Prieto-Mahaney, Y. Terada, T. Yasumoto, T. Shibayama, B. Ohtani, *Chem. Mater.* **2009**, *21*, 2601.
- [32] T. R. Gordon, M. Cargnello, T. Paik, F. Mangolini, R. T. Weber, P. Fornasiero, C. B. Murray, *J. Am. Chem. Soc.* **2012**, *134*, 6751.
- [33] X. Han, Q. Kuang, M. Jin, Z. Xie, L. Zheng, *J. Am. Chem. Soc.* **2009**, *131*, 3152.
- [34] G. Liu, C. Sun, H. G. Yang, S. C. Smith, L. Wang, G. Q. Lu, H. M. Cheng, *Chem. Commun.* **2010**, *46*, 755.
- [35] H. G. Yang, G. Liu, S. Z. Qiao, C. H. Sun, Y. G. Jin, S. C. Smith, J. Zou, H. M. Cheng, G. Q. Lu, *J. Am. Chem. Soc.* **2009**, *131*, 4078.
- [36] W. Yang, J. Li, Y. Wang, F. Zhu, W. Shi, F. Wan, D. Xu, *Chem. Commun.* **2011**, *47*, 1809.
- [37] J. A. Zhu, S. H. Wang, Z. F. Bian, S. H. Xie, C. L. Cai, J. G. Wang, H. G. Yang, H. X. Li, *Cryst. Eng. Comm.* **2010**, *12*, 2219.
- [38] X. H. Yang, Z. Li, C. H. Sun, H. G. Yang, C. Z. Li, *Chem. Mater.* **2011**, *23*, 3486.
- [39] J. Zhang, J. Wang, Z. Zhao, T. Yu, J. Feng, Y. Yuan, Z. Tang, Y. Liu, Z. Li, Z. Zou, *Phys. Chem. Chem. Phys.* **2012**, *14*, 4763.
- [40] W. Wang, C. H. Lu, Y. R. Ni, Z. Z. Xu, *Cryst. Eng. Comm.* **2013**, *15*, 2537.
- [41] W. J. Ong, L. L. Tan, S. P. Chai, S. T. Yong, A. R. Mohamed, *Nanoscale* **2014**, *6*, 1946.
- [42] D. Q. Zhang, G. S. Li, H. B. Wang, K. M. Chan, J. C. Yu, *Cryst. Growth Des.* **2010**, *10*, 1130.
- [43] Y. Alivov, Z. Y. Fan, *J. Phys. Chem. C* **2009**, *113*, 12954.
- [44] J. S. Chen, Y. L. Tan, C. M. Li, Y. L. Cheah, D. Y. Luan, S. Madhavi, F. Y. C. Boey, L. A. Archer, X. W. Lou, *J. Am. Chem. Soc.* **2010**, *132*, 6124.
- [45] L. Mino, F. Pellegrino, S. Rades, J. Radnik, V.-D. Hodoroaba, G. Spoto, V. Maurino, G. Martra, *ACS Appl. Nano Mater.* **2018**, *1*, 5355.
- [46] F. Pellegrino, F. Sordello, L. Mino, C. Minero, V.-D. Hodoroaba, G. Martra, V. Maurino, *ACS Catal.* **2019**, *9*, 6692.
- [47] V. Lavric, R. Isopescu, V. Maurino, F. Pellegrino, L. Pellutiè, E. Ortel, V.-D. Hodoroaba, *Cryst. Growth Des.* **2017**, *17*, 5640.
- [48] R. L. Penn, J. F. Banfield, *Geochim. Cosmochim. Acta* **1999**, *63*, 1549.
- [49] F. Amano, T. Yasumoto, O. O. Prieto-Mahaney, S. Uchida, T. Shibayama, B. Ohtani, *Chem. Commun.* **2009**, *17*, 2311.
- [50] Z. S. Wei, E. Kowalska, B. Ohtani, *Chem. Lett.* **2014**, *43*, 346.
- [51] L. C. Liu, X. R. Gu, Z. Y. Ji, W. X. Zou, C. J. Tang, F. Gao, L. Dong, *J. Phys. Chem. C* **2013**, *117*, 18578.
- [52] C. Deiana, M. Minella, G. Tabacchi, V. Maurino, E. Fois, G. Martra, *Phys. Chem. Chem. Phys.* **2013**, *15*, 307.
- [53] F. Pellegrino, R. Isopescu, L. Pellutiè, F. Sordello, A. M. Rossi, E. Ortel, G. Martra, V.-D., Hodoroaba, V. Maurino, *Sci. Rep.* **2020**, *10*, 18910.
- [54] F. Sordello, F. Pellegrino, M. Prozzi, C. Minero, V. Maurino, *ACS Catal.* **2021**, *11*, 6484.
- [55] J. M. Macak, H. Tsuchiya, A. Ghicov, K. Yasuda, R. Hahn, S. Bauer, P. Schmuki, *Curr. Opin. Solid State Mater. Sci.* **2007**, *11*, 3.
- [56] G. L. Chiarello, A. Zuliani, D. Ceresoli, R. Martinazzo, E. Selli, *ACS Catal.* **2016**, *6*, 1345.
- [57] J. Li, D. Xu, *Chem. Commun.* **2010**, *46*, 2301.
- [58] A. S. Barnard, L. A. Curtiss, *Nano Lett.* **2005**, *5*, 1261.
- [59] C. T. Dinh, T. D. Nguyen, F. Kleitz, T. O. Do, *ACS Nano* **2009**, *3*, 3737.
- [60] J. Pan, G. Liu, G. Q. Lu, H. M. Cheng, *Angew. Chem.* **2011**, *50*, 2133.
- [61] F. Babick, J. Mielke, W. Wohlleben, S. Weigel, V.-D. Hodoroaba, *J. Nanopart. Res.* **2016**, *18*, 158.
- [62] A. Mech, W. Wohlleben, A. Ghanem, V.-D. Hodoroaba, S. Weigel, F. Babick, R. Brüngel, C. M. Friedrich, K. Rasmussen, H. Rauscher, *Small* **2020**, *16*, 2002228.
- [63] C. A. Clifford, E. H. Martins Ferreira, T. Fujimoto, J. Herrmann, A. R. Hight Walker, D. Koltsov, C. Punckt, L. Ren, G. J. Smallwood, A. J. Pollard, *Nat. Rev. Phys.* **2021**, *3*, 233.
- [64] E. Buhr, M. U. Bug, D. Bergmann, P. Cizmar, C. G. Frase, *Meas. Sci. Technol.* **2017**, *28*, 034002.
- [65] L. Crouzier, N. Feltin, A. Delvallée, F. Pellegrino, V. Maurino, G. Cios, T. Tokarski, C. Salzmann, J. Deumer, C. Gollwitzer, V.-D. Hodoroaba, submitted to *Nanomaterials*, MDPI, https://www.mdpi.com/journal/nanomaterials/special_issues/quantification_nanomaterials.
- [66] N. Wollschläger, L. Palasse, I. Häusler, K. Dirscherl, F. Oswald, S. Narbey, E. Ortel, V.-D. Hodoroaba, *Mater. Charact.* **2017**, *131*, 39.
- [67] W. S. Rasband, *ImageJ*, U. S. National Institutes of Health, Bethesda, MD 1997–2018, <https://imagej.nih.gov/ij/>
- [68] E. A. Grulke, K. Yamamoto, K. Kumagai, I. Häusler, W. Österle, E. Ortel, V.-D. Hodoroaba, S. C. Brown, C. Chan, J. Zheng, K. Yamamoto, K. Yashiki, N. W. Song, Y. H. Kim, A. B. Stefaniak, D. Schwegler-Berry, V. A. Coleman, Å. K. Jämting, J. Herrmann, T. Arakawa, W. W. Burchett, J. W. Lambert, A. J. Stromberg, *Adv. Powder Technol.* **2017**, *28*, 1647.
- [69] ISO 21363:2020, *Nanotechnologies — Measurements of Particle Size and Shape Distributions by Transmission Electron Microscopy*, ISO standards Geneva, Switzerland **2020**.
- [70] ISO 19749:2021, *Scanning Electron Microscopy*, ISO standards Geneva, Switzerland **2021**.
- [71] www.bam.de/Content/EN/Projects/nPSize/npsize.html (accessed: November 2021).
- [72] V.-D. Hodoroaba, D. Akcakayiran, D. O. Grigoriev, D. G. Shchukin, *Analyst* **2014**, *139*, 2004.
- [73] J. Mielke, P. Dohányosová, P. Müller, S. López-Vidal, V.-D. Hodoroaba, *Microsc. Microanal.* **2017**, *23*, 163.
- [74] R. Theismann, M. Kluwig, T. Koch, *Beilstein J. Nanotechnol.* **2014**, *5*, 1815.
- [75] K. Kumagai, A. Kurokawa, *Metrologia* **2019**, *56*, 044001.
- [76] F. Bennet, L. Burr, D. Schmid, V.-D. Hodoroaba, *J. Phys.: Conf. Ser.* **2021**, *1953*, 012002.